ELSEVIER

International Journal of Solids and Structures 41 (2004) 4075–4096

INTERNATIONAL JOURNAL OF SOLIDS and STRUCTURES

www.elsevier.com/locate/ijsolstr

A finite element model for the static and dynamic analysis of a piezoelectric bimorph

S.Y. Wang [a,b,*]

[a] *Centre for Advanced Numerical Engineering Simulations, School of Mechanical and Production Engineering, Nanyang Technological University, 50 Nanyang Ave., Singapore 639798, Singapore*

[b] *Singapore-MIT Alliance, 4 Engineering Drive 3, Singapore 117576, Singapore*

Received 18 November 2003; received in revised form 19 February 2004

Available online 9 April 2004

Abstract

A finite element model for the static and dynamic analysis of a piezoelectric bimorph is proposed. It combines a 2D single-layer representation model (finite 2D isoparametric elements) for the mechanical displacement field with a layerwise-like approximation (finite sublayers) for the electric potential field to achieve the accurate prediction of both the mechanical displacement and electric potential fields. Linear through-the-thickness electric potential distribution is assumed only for each piezoelectric sublayer and the actual nonlinear distribution can be reached by using a fine thickness discretization. The unknown induced electric potentials are not included in the global governing equations of motion due to the introduction of an elementary condensation scheme based on the electric boundary conditions and thus the present model will not suffer from an excessive number of potential field variables. A PVDF bimorph beam and a PZT bimorph plate are used to verify the present model. Numerical examples show that the present model can well predict both the global and local responses such as mechanical displacements, modal frequencies as well as the through-the-thickness electric potentials, all in good agreement with those from full 3D finite element model or 3D elasticity theory solution. Furthermore, the conventional piezoelectric finite element models assuming a linear through-the-thickness electric potential field, which is a special case of the present electric potential representation, has been identified as suitable for the global response analysis of thin or moderately thick bimorph plates. The performance of 2D plane models has been evaluated as less accurate in predicting the static and dynamic responses if transversally isotropic piezoelectric materials are involved. The present study may help establish more accurate and efficient piezoelectric models based on better understanding to the piezoelectricity.

Keywords: Finite element method; Piezoelectricity; Piezoelectric bimorph; Single-layer representation; Finite sublayer; Electric potential representation

* Address: Centre for Advanced Numerical Engineering Simulations, School of Mechanical and Production Engineering, Nanyang Technological University, 50 Nanyang Ave., Singapore 639798, Singapore. Tel.: +65-6790-4071; fax: +65-6793-6763.

E-mail address: sywang@ntu.edu.sg (S.Y. Wang).

0020-7683/$ - see front matter © 2004 Elsevier Ltd. All rights reserved.
doi:10.1016/j.ijsolstr.2004.02.058

1. Introduction

Piezoelectric materials have been widely used in many applications. The piezoelectric unimorph and bimorph, which can produce flexural deformation significantly larger than the length or thickness deformation of the individual piezoelectric layers, have been used as electroacoustic transducers, medical devices, microrobot, and atomic force microscope cantilevers due to the characteristics of miniaturization, high positioning accuracy, sensitive response, and large displacement (Ha and Kim, 2002).

The research area of smart/intelligent materials and structures has experienced tremendous growth for decades (Wang, 2002). The promising potential of smart composite structures bonded or embedded with piezoelectric sensors/actuators has triggered intense research interests due to numerous technological applications (Fernandes and Pouget, 2003). The analysis of piezoelectric composite structures such as piezoelectric laminated plates and beams requires efficient and accurate electromechanical modelling of both the mechanical and electric responses such as mechanical displacements and electric potentials. The accurate response of these structures can be obtained by solving the three dimensional (3D) coupled field equations with exact satisfaction of the mechanical and electric boundary conditions and interlaminar continuity conditions (Kapuria, 2001). Exact 3D analytical solutions have been presented for the piezoelectric response of simply supported flat panels and rectangular plates (Ray et al., 1993; Tzou and Tiersten, 1994; Bisegna and Maceri, 1996; Ray et al., 1998). Since the exact 3D analytical solutions are available only for some regular shapes with specified simple boundary conditions, in order that the numerical solution to more general piezoelectric composite structures is possible, the introduction of the finite element method (FEM) is desirable. Finite element (FE) models based on Hamilton's variational principle for piezoelectric composite beams and plates have been reported (Tzou and Tseng, 1990; Hwang and Park, 1993; Lam et al., 1997; Saravanos et al., 1997; Wang et al., 2001; Yao and Lu, 2003). A detailed bibliographical review of the finite element methods applied to the analysis and simulation of smart piezoelectric materials and structures can be found in (Mackerle, 2003). In modelling the mechanical displacement field, the full 3D FE model (Tzou and Tseng, 1990; Yao and Lu, 2003) typically results in large problem size and high computational cost. Several 2D models (1D for beams) with different assumptions made on the through-the-thickness mechanical displacement field distribution are available in the literature (Kapuria, 2001; Fernandes and Pouget, 2003). The equivalent single layer approximations and the layerwise approximations have their own advantages and disadvantages in terms of accuracy, speed of convergence and computational cost and it appears that the single layer approximation based on the first-order shear theory (FOST) can provide a good compromise of solution accuracy, economy, and simplicity (Reddy, 1997).

Furthermore, the through-the-thickness electric potential field distribution can be approximated by various models in the open literature. Mindlin (1952) first made the hypothesis that the electric potential functions have only a constant electric potential across the thickness of the piezoelectric layers. It implies that the electric field along the thickness direction vanish (Bisegna and Caruso, 2001). However, since the thickness direction is usually the poling direction in which the external voltage can be applied, this simplification may cause significant errors. Mindlin (1972) further developed the piezoelectric plate model by assuming that the transversal electric field is constant in the thickness. Hence, the electric potential functions will have a linear variation across the thickness of the piezoelectric layers. This linear transversal electric potential model has been widely adopted (Lee, 1990; Hanagud et al., 1992; Hwang and Park, 1993; Ray et al., 1994; Samanta et al., 1996; Lam et al., 1997; Yang, 1997; Aldraihem and Wetherhold, 1997; Lam and Ng, 1999; Auricchio et al., 2001; Wang et al., 2001; Wang, 2002; Zhu et al., 2002; Kapuria et al., 2003; Wang et al., 2004). As pointed out by Auricchio et al. (2001), this model supplies the exact mean value of the electric potential and may thus be sufficient for most of practical applications. However, as noticed by Yang (1999), this approximation on the electric potential field may be good only for the case of thin actuators. For the piezoelectric closed-circuit sensor, the electric potential in the sensor is neglected by this model and thus the local response of the electric potential field cannot be predicted correctly. After carrying

out a 3D analysis, Bisegna and Maceri (1996) pointed out that the electric potential distribution along the thickness of a piezoelectric layer has a quadratic component and this higher-order electric behavior should be addressed in the piezoelectric plate theories. Yang (1999) showed that this quadratic electric potential variation is directly coupled to the flexure of the actuators and its effect is of the same order as the bending stiffness of the actuators. Although negligible for thin actuators, this effect should be included for thick actuators. It should be noted that in this model the transversal electric field may be linear (Bisegna and Caruso, 2001) or nonlinear in the thickness, depending on whether the higher-order terms is included in the adopted plate theory due to the electromechanical coupling. This quadratic electric potential model has been adopted by a few researchers (Yang, 1999; Gopinathan et al., 2000; Wang and Quek, 2002; Yao and Lu, 2003). Fernandes and Pouget (2003)) further developed this model by adding a half-cosine distribution term to account for the shearing effect. It should also be mentioned that the electric potential functions were initially assumed to have a sinusoidal component by some researchers (Ray et al., 1993, 1998; Lee and Lin, 1998) for the convenience of their trigonometric expansions. To take into account the complex mechanical and electric behavior of the piezoelectric laminate more appropriately, the use of the layerwise theory (Saravanos et al., 1997) or multi-layer modelizations (Bisegna and Caruso, 2001) has been recommended, though it may suffer from an excessive number of field variables in proportion to the number of physical layers or number of distributed sensors and/or actuators. Kapuria (2001) even proposed an electromechanical model that combines the displacement field approximations of the third-order zigzag theory with a layerwise approximation for the electric potential. Furthermore, higher order electrical potential model (up to terms of cubic variation along the actuator thickness) has been proposed by Tiersten (1993) and it is showed that for a very thin plate, the quadratic and cubic terms in the expansion can be ignored. More recently, Bisegna and Caruso (2001) proposed a biquadratic model for the electric potential distribution along the thickness and concluded that in order to obtain accurate estimates of the stress and electric-displacement fields, it is necessary to take into account higher-order terms of up to the fourth-order in the through-the-thickness electric potential representation.

It appears that each electric potential representation model has its own advantages and disadvantages in terms of accuracy and ease of use and computational cost. None of them is generally the best. Bisegna and Caruso (2001) has made a critical comparison to evaluate the higher-order piezoelectric plate theories and it was found that the Lo–Christensen–Wu-type model with biquadratic potential (LCW/B) is able to correctly estimate the leading order terms of the unknowns fields for all the loading conditions considered, which implies that all the existing analytical or FE models may only provide an approximate solutions to the unknown fields and higher-order models can achieve better results. However, further developments on the prescribed higher-order potential models would become less practical due to the much higher computational cost involved. On the other hand, it has been well accepted that the finite element method is a powerful numerical approximate method for the solution of differential and integral equations (Reddy, 1997). Usually, the FEM can guarantee the convergence to the exact solution and better results can be obtained by using a finer mesh. However, in most of the existing FE models for the piezoelectric laminated plates, the mechanical displacement and electric potential fields are discretized in the 2D midplane only, while the through-the-thickness electric potential is assumed to be linear and thus no discretization is introduced in the thickness (Hwang and Park, 1993; Samanta et al., 1996; Lam et al., 1997; Aldraihem and Wetherhold, 1997; Lam and Ng, 1999; Wang et al., 1999; Auricchio et al., 2001; Wang et al., 2001; Wang, 2002; Zhu et al., 2002; Wang et al., 2004, 2003). Hence, it is evident that there is an inconsistency in the FEM. Since the electric field can affect the mechanical response significantly through the electromechanical coupling, there is no guarantee that both the mechanical displacement and electric potential fields converge to the exact solution with the use of finer meshes and the numerical results may depend on the assumed through-the-thickness distribution of the electric potential heavily.

The objective of the present study is to establish an efficient FE model to overcome the drawback of the inconsistent FEM methodology. Both the unknown mechanical displacement and electric potential fields

are discretized. In addition to the 2D discretization of the mechanical displacement field in the midplane, the electric potential field of each piezoelectric sensor and/or actuator layer is further discretized by finite sublayers. This FE model combines a 2D single-layer representation model for the mechanical displacement field with a 3D layerwise-like approximation for the electric potential field and is capable of predicting both the global and local responses of a thin or moderately thick piezoelectric bimorph accurately.

2. Formulation of the piezoelectric finite element modelling

Fig. 1 shows the geometry of a piezoelectric bimorph. The bimorph structure undergoing the action of the external mechanical and electric forces (a uniformly distributed surface load P_s and an applied electric voltage of V_0) is assumed to be perfectly bonded, elastic and orthotropic in behavior (Kekana, 2002) with small strains and displacements (Wang et al., 2004). The deformation of the bimorph is assumed to take place under isothermal conditions. Moreover, the piezoelectric sensors/actuators are made of homogenous and isotropic dielectric materials (Cheng, 1989) and high electric fields and cyclic fields are not involved (Ehlers and Weisshaar, 1990). Based on these assumptions, a linear constitutive relationship (Wang, 2002) is employed for the static and dynamic analysis of the piezoelectric bimorph.

2.1. Linear piezoelectric constitutive equations

The linear piezoelectric constitutive equations (LPCE) in Voigt notation can be expressed as

$$\boldsymbol{\sigma} = \mathbf{c}\varepsilon - \mathbf{e}^{\mathrm{T}}\mathbf{E}, \tag{1}$$

$$\mathbf{D} = \mathbf{e}\varepsilon + \mathbf{g}\mathbf{E}, \tag{2}$$

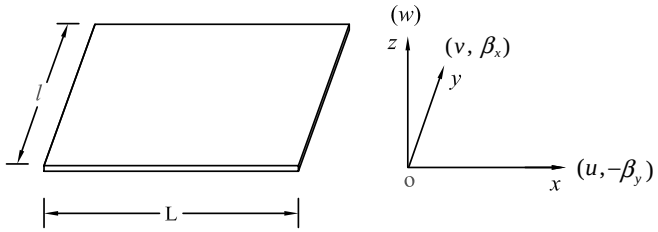

(a) Coordinate denotation

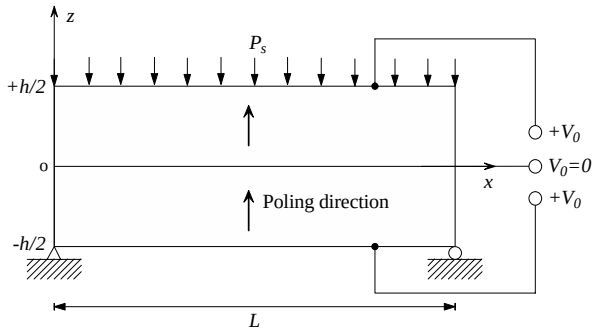

(b) Side view

Fig. 1. Geometry of a piezoelectric bimorph.

where $\boldsymbol{\sigma}$ is the stress vector; $\mathbf{c}$ the elasticity matrix; ε the strain vector; $\mathbf{e}$ the piezoelectric constant matrix; $\mathbf{E}$ the electric field vector; $\mathbf{D}$ the electric displacement vector; and $\mathbf{g}$ the dielectric constant matrix. Eqs. (1) and (2) represent the converse and direct piezoelectric effects (Tzou and Tseng, 1990), respectively.

Furthermore, the magnetically static electric field vector $\mathbf{E}$ in the LPCE is related to the electric potential field ϕ by using a gradient vector $\bigtriangledown$ (Tzou and Tseng, 1990) as

$$\mathbf{E} = -\bigtriangledown \phi. \tag{3}$$

2.2. Variational form of the governing equations of motion

The governing equations of motion of the piezoelectric bimorph plate can be derived by using Hamilton's variational principle (Hwang and Park, 1993), which can be written as

$$\boldsymbol{\delta} \int_{t_1}^{t_2} (T - U + W)\,\mathrm{d}t = 0, \tag{4}$$

where t_1 and t_2 are the starting and finish time, respectively; T the total kinetic energy; U the total potential energy; and W the total work done by the external mechanical and electrical forces. The total kinetic energy T for the volume Ω of the bimorph plate is given (Wang, 2002) as

$$T = \frac{1}{2} \int_{\Omega} \dot{\mathbf{u}}^{\mathrm{T}} \rho \dot{\mathbf{u}}\,\mathrm{d}\Omega, \tag{5}$$

where $\dot{\mathbf{u}}$ is the velocity field vector and ρ the mass density. The total potential energy U, including the mechanical strain and electrical potential energies, is given (Tzou and Tseng, 1990) as

$$U = \frac{1}{2} \int_{\Omega} (\boldsymbol{\sigma}^{\mathrm{T}} \varepsilon - \mathbf{E}^{\mathrm{T}} \mathbf{D})\,\mathrm{d}\Omega. \tag{6}$$

The total work W done by the external mechanical and electrical forces is given (Tzou, 1993) as

$$W = \int_{\Omega} \mathbf{u}^{\mathrm{T}} \mathbf{P}_{\mathrm{b}}\,\mathrm{d}\Omega + \int_{\Gamma_{\mathrm{s}}} \mathbf{u}^{\mathrm{T}} \mathbf{P}_{\mathrm{s}}\,\mathrm{d}\Gamma_{\mathrm{s}} + \sum_i \mathbf{u}_i^{\mathrm{T}} \mathbf{P}_i - \int_{\Gamma_\phi} \phi q_0\,\mathrm{d}\Gamma_\phi, \tag{7}$$

where $\mathbf{u}$ is the displacement field vector, $\mathbf{P}_{\mathrm{b}}$, $\mathbf{P}_{\mathrm{s}}$ and $\mathbf{P}_i$ the body, surface and ith concentrated load vectors, respectively; q_0 the surface charge density; Γ_{s} the external mechanical loading surface; and Γ_ϕ the external electrical loading surface. Substituting Eqs. (5)–(7) and (1)–(3) into Eq. (4) and applying the condition that all variations must vanish at the times $t = t_1$ and $t = t_2$ will yield the governing equations of motion in variational form as follows:

$$\begin{aligned} &\int_{\Omega} (\boldsymbol{\delta}\mathbf{u}^{\mathrm{T}} \rho \ddot{\mathbf{u}} + (\mathbf{L}\boldsymbol{\delta}\mathbf{u})^{\mathrm{T}} \mathbf{C} \mathbf{L}\mathbf{u} + (\mathbf{L}\boldsymbol{\delta}\mathbf{u})^{\mathrm{T}} \mathbf{e}^{\mathrm{T}} \bigtriangledown \phi + (\bigtriangledown \boldsymbol{\delta}\phi)^{\mathrm{T}} \mathbf{e} \mathbf{L}\mathbf{u} - (\bigtriangledown \boldsymbol{\delta}\phi)^{\mathrm{T}} \mathbf{g} \bigtriangledown \phi - \boldsymbol{\delta}\mathbf{u}^{\mathrm{T}} \mathbf{P}_{\mathrm{b}})\mathrm{d}\Omega \\ &\quad - \int_{\Gamma_{\mathrm{s}}} \boldsymbol{\delta}\mathbf{u}^{\mathrm{T}} \mathbf{P}_{\mathrm{s}} \mathrm{d}\Gamma_{\mathrm{s}} - \sum_i \boldsymbol{\delta}\mathbf{u}_i^{\mathrm{T}} \mathbf{P}_i + \int_{\Gamma_\phi} q_0 \boldsymbol{\delta}\phi \mathrm{d}\Gamma_\phi = 0, \end{aligned} \tag{8}$$

in which the strain vector ε is represented as $\varepsilon = \mathbf{L}\mathbf{u}$, where $\mathbf{L}$ represents a matrix of differential operator (Kekana, 2002).

In the above variational form of governing equations of motion Eq. (8), the mechanical displacement field $\mathbf{u}$ and electric potential field ϕ are the unknown functions. To solve these unknowns numerically, an efficient FE model will be established in the present study by adopting the approximations on the through-the-thickness mechanical displacement and electric potential fields, as next discussed.

2.3. Approximations on the mechanical displacements

In the present single-layer representation for the mechanical displacements, the plate theory FOST is adopted. The mechanical displacements of a bimorph plate based on the FOST takes the following form (Wang et al., 2001):

$$\begin{aligned} u(x,y,z,t) &= u_0(x,y,t) + z\beta_x(x,y,t), \\ v(x,y,z,t) &= v_0(x,y,t) + z\beta_y(x,y,t), \\ w(x,y,z,t) &= w_0(x,y,t), \end{aligned} \tag{9}$$

where u_0, v_0, w_0 are the components of the displacement vector $\mathbf{u}(x,y,0)$ of a reference point $(x,y,0)$ at the midplane $(z=0)$ along the x,y,z axes, respectively; u,v,w the components of the displacement vector $\mathbf{u}(x,y,z)$ of any point (x,y,z) in the plate along the x,y,z axes, respectively; and β_x, β_y the slopes of the normal to the reference point $(x,y,0)$ on the midplane in the yz, xz planes, respectively, as depicted in Fig. 1(a). It should be noted that the rotations β_x and β_y are different from the right-hand-rule rotations and may greatly simplify the algebra involved (Hughes, 1987). Eq. (9) can also be expressed in matrix form as

$$\mathbf{u} = \widehat{\mathbf{Z}}\mathbf{u}_0, \tag{10}$$

where

$$\widehat{\mathbf{Z}} = \begin{bmatrix} 1 & 0 & 0 & z & 0 \\ 0 & 1 & 0 & 0 & z \\ 0 & 0 & 1 & 0 & 0 \end{bmatrix}, \tag{11}$$

$$\mathbf{u}_0 = \begin{bmatrix} u_0 & v_0 & w_0 & \beta_x & \beta_y \end{bmatrix}^{\mathrm{T}}. \tag{12}$$

Based on the FOST, the relationship between the strains at any point along the thickness direction and those at the mid-surface can be written as follows:

$$\begin{aligned} &\varepsilon_i(x,y,z,t) = \varepsilon_i^0(x,y,t) + z\kappa_i^0 \quad (i=1,2,6), \\ &\varepsilon_3(x,y,z,t) = 0, \\ &\varepsilon_i(x,y,z,t) = \varepsilon_i^0(x,y,t) \quad (i=4,5), \end{aligned} \tag{13}$$

where ε_i is linear strains for small deformations of any point in the plate, and ε_i^0, κ_i^0 the corresponding strains and curvatures of the plate at the midplane, respectively, which can be written (Saravanos et al., 1997) as

$$\begin{aligned} &\varepsilon_1^0 = \frac{\partial u_0}{\partial x}, \quad \varepsilon_2^0 = \frac{\partial v_0}{\partial y}, \quad \varepsilon_3^0 = 0, \\ &\varepsilon_4^0 = \beta_y + \frac{\partial w_0}{\partial y}, \quad \varepsilon_5^0 = \beta_x + \frac{\partial w_0}{\partial x}, \quad \varepsilon_6^0 = \frac{\partial u_0}{\partial y} + \frac{\partial v_0}{\partial x}, \\ &\kappa_1^0 = \beta_{x,x}, \quad \kappa_2^0 = \beta_{y,y}, \quad \kappa_6^0 = \beta_{x,y} + \beta_{y,x}. \end{aligned} \tag{14}$$

According to Eqs. (10), (13) and (14), the mechanical displacements and strains at any point in the bimorph 3D space can be obtained from the displacement vector in the 2D midplane. This reduction of a 3D problem into a 2D problem can greatly simplify the computational analysis. In this study, the quadratic eight-noded isoparametric element in (Wang et al., 2001; Wang, 2002) is adopted to discretize the 2D midplane and thus for an element, the continuous mechanical displacement vector $\mathbf{u}_0$ can be approximated by using the finite element shape functions as

$$\mathbf{u}_0 = \mathbf{N}_u \tilde{\mathbf{u}}^e, \tag{15}$$

where $\mathbf{N}_u$ is the matrix of displacement shape functions, $\tilde{\mathbf{u}}^e$ the discrete element nodal displacement vector (Wang, 2002).

Hence, the corresponding mechanical displacements and strains of any point in the 3D plate space can be obtained as

$$\mathbf{u} = \widehat{\mathbf{Z}} \mathbf{N}_u \tilde{\mathbf{u}}^e, \tag{16}$$

$$\varepsilon = \mathbf{L}\mathbf{u} = \mathbf{Z}\mathbf{B}_u \tilde{\mathbf{u}}^e \tag{17}$$

in which the thickness coordinate matrix $\mathbf{Z}$ and the strain–displacement matrix $\mathbf{B}_u$ are defined in (Wang et al., 2001; Wang, 2002).

2.4. Approximations on the electric potentials

In the present study, approximations on the electric potential field of each piezoelectric layer are made by further discretization of each piezoelectric layer into finite sublayers along the thickness direction and assuming a linear through-the-thickness electric potential distribution for each piezoelectric sublayer. It can be expected that the actual electric potential field of each piezoelectric sensor and/or actuator layer can be approached with more sublayers for the layer and thus the convergence of both the mechanical displacement and electric potential fields to a better solution can be ensured. Hence, this piezoelectric FE model, which combines a 2D FOST model (equivalent single-layer representation (Fernandes and Pouget, 2003)) for the mechanical displacement field with a layerwise-like approximation for the electric potential field, would be able to achieve the convergence of both the unknown mechanical displacement and electric potential fields. Furthermore, any higher-order hypothesis on the actual through-the-thickness electric potential field of each piezoelectric sensor and/or actuator layer is not needed.

Fig. 2 shows that each layer of the piezoelectric bimorph is discretized by n_{sub} sublayers in the thickness to model the actual through-the-thickness distribution of the electric potential. It is assumed that each sublayer has a linear electric potential function $\phi^i(z), (i = 1, 2, \ldots, 2n_{\text{sub}})$ across the thickness as

$$\phi^i(z) = \mathbf{N}_\phi^i \tilde{\boldsymbol{\phi}}^i \tag{18}$$

in which $\mathbf{N}_\phi^i$ is the shape function of the electric potential function and $\tilde{\boldsymbol{\phi}}^i$ the electric potentials at the top and bottom surfaces of the sublayer, which can be expressed as

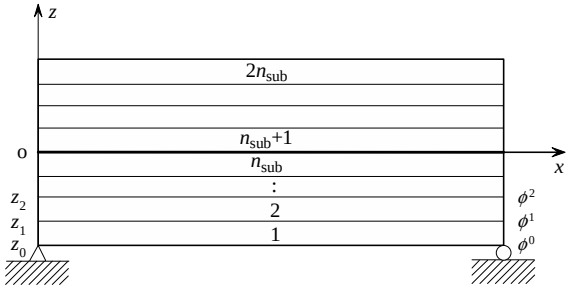

Fig. 2. Finite sublayers of a piezoelectric bimorph.

$$\mathbf{N}_{\phi}^{i} = \frac{1}{h_i}[\, z_i - z \quad z - z_{i-1}\,], \qquad h_i = z_i - z_{i-1}, \qquad z_{i-1} \leqslant z \leqslant z_i, \tag{19}$$

$$\tilde{\boldsymbol{\phi}}^{i} = \begin{Bmatrix} \phi^{i-1} \\ \phi^{i} \end{Bmatrix}. \tag{20}$$

Hence, the conventional linear through-the-thickness electric potential model is only a special case of the present model, $n_{\text{sub}} = 1$, and therefore comparative study can be easily carried out. The same global 2D mesh for the midplane is also used to discretize each piezoelectric sublayer in the xy plane to keep the compatibility. For each piezoelectric sublayer element, it is assumed that the electric potentials at the same height along the thickness are the same, as recommended in (Hwang and Park, 1993; Wang et al., 2001). Since in practice the surfaces of piezoelectric sensors and actuators are usually electroplated (Lee, 1987, 1990), the variation of the electric potential in the xy plane is insignificant and more importantly, the error caused by this approximation can be reduced by using a fine mesh, as demonstrated by Hwang and Park (1993). Hence, for each discretized sublayer element, the electric field $\mathbf{E}$ in Eq. (3) can be re-written as

$$\mathbf{E}^{i} = \mathbf{B}_{\phi}^{i}\tilde{\boldsymbol{\phi}}^{i}, \tag{21}$$

where

$$\mathbf{B}_{\phi}^{i} = \frac{1}{h_i}\begin{bmatrix} 0 & 0 \\ 0 & 0 \\ 1 & -1 \end{bmatrix}. \tag{22}$$

2.5. Elementary governing equations of motion

The elementary governing equations of motion can be derived by substituting Eqs. (16)–(18) and (21) into Eq. (8) and assembling the electric potentials along the thickness, which can be written as follows:

$$\mathbf{M}^{\mathrm{e}}\ddot{\tilde{\mathbf{u}}}^{\mathrm{e}} + \mathbf{K}_{uu}^{\mathrm{e}}\tilde{\mathbf{u}}^{\mathrm{e}} - \mathbf{K}_{u\phi}^{\mathrm{e}}\tilde{\boldsymbol{\phi}}^{\mathrm{e}} = \mathbf{f}^{\mathrm{e}}, \tag{23}$$

$$\mathbf{K}_{\phi u}^{\mathrm{e}}\tilde{\mathbf{u}}^{\mathrm{e}} + \mathbf{K}_{\phi\phi}^{\mathrm{e}}\tilde{\boldsymbol{\phi}}^{\mathrm{e}} = \mathbf{q}^{\mathrm{e}}, \tag{24}$$

where $\mathbf{M}^{\mathrm{e}}$ is the elementary mass matrix; $\mathbf{K}_{uu}^{\mathrm{e}}$ mechanical stiffness matrix; $\mathbf{K}_{u\phi}^{\mathrm{e}}$ and $\mathbf{K}_{\phi u}^{\mathrm{e}}$ the piezoelectric coupling matrices; $\mathbf{K}_{\phi\phi}^{\mathrm{e}}$ the dielectric primitivity matrix; $\tilde{\boldsymbol{\phi}}^{\mathrm{e}}$ the discrete elementary electric voltage vector; $\mathbf{f}^{\mathrm{e}}$ the nodal external force vector; and $\mathbf{q}^{\mathrm{e}}$ the nodal externally applied charge vector.

$$\mathbf{M}^{\mathrm{e}} = \int_{\Omega_{\mathrm{e}}} \mathbf{N}_{u}^{\mathrm{T}}\widehat{\mathbf{Z}}^{\mathrm{T}}\rho\widehat{\mathbf{Z}}\mathbf{N}_{u}\,\mathrm{d}\Omega, \tag{25}$$

$$\mathbf{K}_{uu}^{e} = \int_{\Omega_{\mathrm{e}}} \mathbf{B}_{u}^{\mathrm{T}}\mathbf{Z}^{\mathrm{T}}\mathbf{c}\mathbf{Z}\mathbf{B}_{u}\,\mathrm{d}\Omega, \tag{26}$$

$$\mathbf{K}_{u\phi}^{i} = -\int_{\Omega_i} \mathbf{B}_{u}^{\mathrm{T}}\mathbf{Z}^{\mathrm{T}}\mathbf{e}^{\mathrm{T}}\mathbf{B}_{\phi}^{i}\,\mathrm{d}\Omega = -h_i\int_{\Gamma_i} \mathbf{B}_{u}^{\mathrm{T}}\mathbf{Z}_{i}^{\mathrm{T}}\mathbf{e}^{\mathrm{T}}\mathbf{B}_{\phi}^{i}\,\mathrm{d}\Gamma, \tag{27}$$

$$\mathbf{K}_{\phi u}^{i} = (\mathbf{K}_{u\phi}^{i})^{\mathrm{T}}, \tag{28}$$

$$\mathbf{K}_{\phi u}^{\mathrm{e}} = \sum_{i}\mathbf{K}_{\phi u}^{i} = (\mathbf{K}_{u\phi}^{\mathrm{e}})^{\mathrm{T}}, \tag{29}$$

$$\mathbf{K}^i_{\phi\phi} = \int_{\Omega_i} (\mathbf{B}^i_\phi)^{\mathrm{T}} \mathbf{g} \mathbf{B}^i_\phi \, \mathrm{d}\Omega = \frac{1}{h_i} \int_{\Gamma_i} g_{33} \begin{bmatrix} 1 & -1 \\ -1 & 1 \end{bmatrix} \mathrm{d}\Gamma, \tag{30}$$

$$\mathbf{K}^{\mathrm{e}}_{\phi\phi} = \sum_i \mathbf{K}^i_{\phi\phi}, \tag{31}$$

$$\tilde{\boldsymbol{\phi}}^{\mathrm{e}} = \begin{bmatrix} \phi^0 & \phi^1 & \dots & \phi^{2n_{\mathrm{sub}}} \end{bmatrix}^{\mathrm{T}}, \tag{32}$$

$$\mathbf{f}^{\mathrm{e}} = \int_{\Omega_{\mathrm{e}}} \mathbf{N}_u^{\mathrm{T}} \widehat{\mathbf{Z}}^{\mathrm{T}} \mathbf{P}_{\mathrm{b}} \mathrm{d}\Omega + \int_{\Gamma^{\mathrm{e}}_{\mathrm{s}}} \mathbf{N}_u^{\mathrm{T}} \mathbf{P}_{\mathrm{s}} \mathrm{d}\Gamma_{\mathrm{s}} + \sum_i \mathbf{N}_{ui}^{\mathrm{T}} \mathbf{P}^{\mathrm{e}}_i, \tag{33}$$

$$\mathbf{q}^{\mathrm{e}} = \sum_i \int_{\Gamma^i_\phi} (\mathbf{N}^i_\phi)^{\mathrm{T}} \mathbf{q}_0 \mathrm{d}\Gamma_\phi, \tag{34}$$

where Ω_i is the ith piezoelectric sublayer domain, Γ_i the mid-surface of the sublayer, and $\mathbf{Z}_i$ the coordinate matrix at Γ_i.

2.6. Static condensation by matrix algebra

Two sets of governing equations of motion corresponding to the external mechanical forces and electric charges have been derived, as shown in Eqs. (23) and (24). It should be noted that the charge equation Eq. (24), which implies that the total of the electric flux out of the surfaces of an element is equal to the electric charge enclosed, is equivalent to the Gauss's law (Wang, 2002), or Maxwell's first equation. After the global matrices are assembled, the vectors of unknown displacements and potentials would be directly solved for. However, for the piezoelectric materials, typical element values of $\mathbf{K}^{\mathrm{e}}_{uu}$ are of the order 10^8, while typical element values of $\mathbf{K}^{\mathrm{e}}_{\phi\phi}$ are of the order 10^{-11}. This huge difference in magnitudes would make the global matrices too ill conditioned if the two governing equations of motion are taken as a whole. To overcome this problem, the general method of static condensation by matrix algebra can be adopted. In the present study, the unknown potentials are sacrificed in favor of the unknown displacements. The governing equations of motions Eqs. (23) and (24) are finally condensed as

$$\mathbf{M}^{\mathrm{e}} \ddot{\tilde{\mathbf{u}}}^{\mathrm{e}} + (\mathbf{K}^{\mathrm{e}}_{uu} + \mathbf{K}^{\mathrm{e}}_{\mathrm{p}}) \tilde{\mathbf{u}}^{\mathrm{e}} = \mathbf{f}^{\mathrm{e}} + \mathbf{f}^{\mathrm{e}}_{\mathrm{a}}, \tag{35}$$

where $\mathbf{K}^{\mathrm{e}}_{\mathrm{p}}$ is the induced mechanical stiffness matrix due to the electromechanical coupling of the piezoelectric materials, $\mathbf{f}^{\mathrm{e}}_{\mathrm{a}}$ the equivalent (induced) mechanical forces of the applied voltages of piezoelectric actuators, which can be given as

$$\mathbf{f}^{\mathrm{e}}_{\mathrm{a}} = \sum_k \mathbf{f}^k_{\mathrm{a}}, \tag{36}$$

where $\mathbf{f}^k_{\mathrm{a}}$ is the equivalent force vector of the kth actuator, which will be discussed later.

It should be highlighted that the calculation of the induced mechanical stiffness matrix $\mathbf{K}^{\mathrm{e}}_{\mathrm{p}}$ is generally complicated since the elementary dielectric primitivity matrix $\mathbf{K}^{\mathrm{e}}_{\phi\phi}$ in Eq. (24) is not positive definite. To make this static condensation possible, electric boundary conditions must be applied such that the reduced elementary dielectric primitivity matrix will be positive definite and the unknown potentials can be solved in terms of the elementary displacements from Eq. (24). Since the piezoelectric materials can be used as sensors either in closed circuit or in open circuit and/or actuators, three different electric boundary conditions have to be considered. Hence, $\mathbf{K}^{\mathrm{e}}_{\mathrm{p}}$ can be given as

$$\mathbf{K}_{\mathrm{p}}^{\mathrm{e}} = \sum_i \mathbf{K}_{\mathrm{c}}^i + \sum_j \mathbf{K}_{\mathrm{o}}^j + \sum_k \mathbf{K}_{\mathrm{a}}^k, \tag{37}$$

where $\mathbf{K}_{\mathrm{c}}^i$, $\mathbf{K}_{\mathrm{o}}^j$ and $\mathbf{K}_{\mathrm{a}}^k$ are the corresponding induced stiffness of the piezoelectric sensor in closed circuit, the sensor in open circuit and the piezoelectric actuator, respectively, which will be given as follows.

2.6.1. Case I: Piezoelectric sensor in closed circuit

For the kth piezoelectric closed circuit sensor, since the electric potentials at the top and bottom surfaces of the sensor layer are zero (grounded) (Lee, 1990), the electric potential vector becomes $\tilde{\boldsymbol{\phi}}^k = \begin{bmatrix} 0 & \tilde{\boldsymbol{\phi}}_{\mathrm{c}}^k & 0 \end{bmatrix}^{\mathrm{T}}$, where $\tilde{\boldsymbol{\phi}}_{\mathrm{c}}^k$ is the induced sensor potential vector. Furthermore, since it is assumed that there is no free charge inside the piezoelectric materials, after the standard FEM assemblage of the charge equation of each sublayer of the sensor layer, the electric charges at the top and bottom surfaces of the finite sublayers inside the sensor layer must vanish, except at the top and bottom surfaces of the sensor layer. According to Eq. (24), the corresponding charge equation for the kth sensor can be written as

$$\mathbf{K}_{\phi u}^k \tilde{\mathbf{u}}^{\mathrm{e}} + \mathbf{K}_{\phi\phi}^k \begin{Bmatrix} 0 \\ \tilde{\boldsymbol{\phi}}_{\mathrm{c}}^k \\ 0 \end{Bmatrix} = \begin{Bmatrix} q_0^k \\ \mathbf{0} \\ q_{n_{\mathrm{sub}}}^k \end{Bmatrix}, \tag{38}$$

where $\tilde{\boldsymbol{\phi}}_{\mathrm{c}}^k$ can be obtained by solving Eq. (38) as

$$\tilde{\boldsymbol{\phi}}_{\mathrm{c}}^k = -(\mathbf{K}_{\phi\phi}^{\mathrm{c}})^{-1} \mathbf{K}_{\phi u}^{\mathrm{c}} \tilde{\mathbf{u}}^{\mathrm{e}} \tag{39}$$

in which $\mathbf{K}_{\phi\phi}^{\mathrm{c}}$ and $\mathbf{K}_{\phi u}^{\mathrm{c}}$ are the corresponding submatrices of $\mathbf{K}_{\phi\phi}^k$ and $\mathbf{K}_{\phi u}^k$, respectively. Since the induced electric potentials can be expressed by the elementary nodal displacements $\tilde{\mathbf{u}}^{\mathrm{e}}$, the governing equations in Eqs. (23) and (24) can be reduced in terms of $\tilde{\mathbf{u}}^{\mathrm{e}}$ only. According to Eqs. (23) and (24), the electrically induced stiffness of the piezoelectric closed-circuit sensor $\mathbf{K}_{\mathrm{c}}^k$ can be written as

$$\mathbf{K}_{\mathrm{c}}^k = -\mathbf{K}_{u\phi}^k \tilde{\boldsymbol{\phi}}^k = (\mathbf{K}_{\phi u}^{\mathrm{c}})^{\mathrm{T}} (\mathbf{K}_{\phi\phi}^{\mathrm{c}})^{-1} \mathbf{K}_{\phi u}^{\mathrm{c}}. \tag{40}$$

It should be noted that different from most of the finite element models (Hwang and Park, 1993; Ray et al., 1994; Samanta et al., 1996; Lam et al., 1997; Aldraihem and Wetherhold, 1997; Wang et al., 2001; Wang, 2002; Zhu et al., 2002) and some of the analytical models (Lee, 1987, 1990; Hanagud et al., 1992; Yang, 1997; Lam and Ng, 1999; Auricchio et al., 2001), the induced sensor potentials do not vanish in the present FEM model and thus the induced stiffness $\mathbf{K}_{\mathrm{c}}^k$ due to the electromechanical coupling can be taken into account accurately.

2.6.2. Case II: Piezoelectric sensor in open circuit

For the kth piezoelectric open circuit sensor, the electric potential at the bottom surface of the sensor layer can be assumed as zero (grounded) and thus the electric potential vector becomes $\tilde{\boldsymbol{\phi}}^k = \begin{bmatrix} 0 & \tilde{\boldsymbol{\phi}}_{\mathrm{o}}^k \end{bmatrix}^{\mathrm{T}}$, where $\tilde{\boldsymbol{\phi}}_{\mathrm{o}}^k$ is the induced open-circuit sensor potential vector. Similarly, the corresponding charge equation for the open circuit sensor can be derived as

$$\mathbf{K}_{\phi u}^k \tilde{\mathbf{u}}^{\mathrm{e}} + \mathbf{K}_{\phi\phi}^k \begin{Bmatrix} 0 \\ \tilde{\boldsymbol{\phi}}_{\mathrm{o}}^k \end{Bmatrix} = \begin{Bmatrix} q_0^k \\ \mathbf{0} \end{Bmatrix}, \tag{41}$$

where $\tilde{\boldsymbol{\phi}}_{\mathrm{o}}^k$ can be obtained by solving Eq. (41) as given by

$$\tilde{\boldsymbol{\phi}}_{\mathrm{o}}^k = -(\mathbf{K}_{\phi\phi}^{\mathrm{o}})^{-1} \mathbf{K}_{\phi u}^{\mathrm{o}} \tilde{\mathbf{u}}^{\mathrm{e}} \tag{42}$$

in which $\mathbf{K}_{\phi\phi}^{\mathrm{o}}$ and $\mathbf{K}_{\phi u}^{\mathrm{o}}$ are the corresponding submatrices of $\mathbf{K}_{\phi\phi}^k$ and $\mathbf{K}_{\phi u}^k$, respectively. Hence, the induced stiffness of the piezoelectric open-circuit sensor $\mathbf{K}_{\mathrm{o}}^k$ can be written as

$$\mathbf{K}_{\mathrm{o}}^{k} = -\mathbf{K}_{u\phi}^{k}\tilde{\boldsymbol{\phi}}^{k} = (\mathbf{K}_{\phi u}^{\mathrm{o}})^{\mathrm{T}}(\mathbf{K}_{\phi\phi}^{\mathrm{o}})^{-1}\mathbf{K}_{\phi u}^{\mathrm{o}}. \tag{43}$$

Comparing Eqs. (42) with (39) and Eqs. (43) with (40), it appears that induced electric potential and stiffness of the piezoelectric sensor in open circuit are similar to those in closed circuit. However, after comparing Eqs. (41) with (38), it can be found that the magnitude of $\tilde{\boldsymbol{\phi}}_{\mathrm{o}}^{k}$ and $\mathbf{K}_{\mathrm{o}}^{k}$ will be significantly larger than that of $\tilde{\boldsymbol{\phi}}_{\mathrm{c}}^{k}$ and $\mathbf{K}_{\mathrm{c}}^{k}$, since the constraints on the induced electric potential for the sensor in closed circuit is much more severe than in open circuit.

2.6.3. Case III: Piezoelectric actuator

For the kth piezoelectric actuator with an applied voltage of V^{k}, it can be assumed that the electric potential is zero (grounded) at the bottom surface of the actuator layer and V^{k} at the top surface. Hence, the electric potential vector becomes $\tilde{\boldsymbol{\phi}}^{k} = \begin{bmatrix} 0 & \tilde{\boldsymbol{\phi}}_{\mathrm{a}}^{k} & V^{k} \end{bmatrix}^{\mathrm{T}}$, where $\tilde{\boldsymbol{\phi}}_{\mathrm{a}}^{k}$ is the induced actuator potential vector. The corresponding charge equation for the piezoelectric actuator can be derived as

$$\mathbf{K}_{\phi u}^{k}\tilde{\mathbf{u}}^{\mathrm{e}} + \mathbf{K}_{\phi\phi}^{k}\begin{Bmatrix} 0 \\ \tilde{\boldsymbol{\phi}}_{\mathrm{a}}^{k} \\ V^{k} \end{Bmatrix} = \begin{Bmatrix} q_{0}^{k} \\ \mathbf{0} \\ q_{n_{\mathrm{sub}}}^{k} \end{Bmatrix} \tag{44}$$

Hence, $\tilde{\boldsymbol{\phi}}_{\mathrm{a}}^{k}$ can be obtained as

$$\tilde{\boldsymbol{\phi}}_{\mathrm{a}}^{k} = -(\mathbf{K}_{\phi\phi}^{\mathrm{a}})^{-1}\mathbf{K}_{\phi u}^{\mathrm{a}}\tilde{\mathbf{u}}^{\mathrm{e}} - (\mathbf{K}_{\phi\phi}^{\mathrm{a}})^{-1}\mathbf{K}_{\phi\phi,1}^{\mathrm{a}}V^{k} \tag{45}$$

in which $\mathbf{K}_{\phi\phi}^{\mathrm{a}}$ and $\mathbf{K}_{\phi u}^{\mathrm{a}}$ are the corresponding submatrices of $\mathbf{K}_{\phi\phi}^{k}$ and $\mathbf{K}_{\phi u}^{k}$, respectively, and $\mathbf{K}_{\phi\phi,1}^{\mathrm{a}}$ is the first column of the corresponding submatrices of $\mathbf{K}_{\phi\phi}^{k}$. Comparing Eq. (45) with Eq. (39), it can be found that the first term of the right side of Eq. (45) is similar to the nonlinear induced potentials of a closed-circuit sensor, with the same constraints on the potentials at the top and bottom surfaces. Furthermore, the second term is independent of the unknown displacement field. It should be noted that, without the electromechanical coupling, the applied voltage V^{k} would lead to a linear through-the-thickness distribution of the electric potentials. Therefore, the actual through-the-thickness distribution of the electric potentials is the summation of the linear distribution induced by the applied voltage directly and the nonlinear distribution induced by the electromechanical coupling. Since the latter is secondary compared with the former, in most cases the actual through-the-thickness distribution of the electric potentials of the piezoelectric actuators may be approximated as linear, especially for thin or moderately thick plates. Closed-form solutions of Fernandes and Pouget (2003) for a thick plate with an aspect ratio of 5 also suggest that through the thickness, the electric potential function would be linear and the electric field constant. Similar observation can also be found in Gopinathan et al. (2000), in which it is shown that the constant electric field model for the piezoelectric actuators predicts results similar to the 3D elastic solution. According to the present FE model, those solutions can be reasonable since the nonlinear potential response may usually be insignificant. Hence, though less accurate for the piezoelectric sensors, the linear through-the-thickness electric potential field model adopted by most FE models (Hwang and Park, 1993; Ray et al., 1994; Samanta et al., 1996; Lam et al., 1997; Aldraihem and Wetherhold, 1997; Wang et al., 2001; Wang, 2002; Zhu et al., 2002) and the analytical models (Lee, 1990; Hanagud et al., 1992; Yang, 1997;Lam and Ng, 1999; Auricchio et al., 2001) may be able to obtain fairly good results for the piezoelectric actuators.

Hence, the induced stiffness of the piezoelectric actuator $\mathbf{K}_{\mathrm{a}}^{k}$ can be written as

$$\mathbf{K}_{\mathrm{a}}^{k} = (\mathbf{K}_{\phi u}^{\mathrm{a}})^{\mathrm{T}}(\mathbf{K}_{\phi\phi}^{\mathrm{a}})^{-1}\mathbf{K}_{\phi u}^{\mathrm{a}}. \tag{46}$$

Comparing Eq. (46) with Eq. (40), it can be found that the induced stiffness for these two cases are similar since the nonlinear induced potentials are the same. The equivalent mechanical force vector $\mathbf{f}_{\mathrm{a}}^{k}$ of the applied voltage of the piezoelectric actuator can be given as

$$\mathbf{f}_{\mathrm{a}}^{k} = -(\mathbf{K}_{\phi u}^{\mathrm{a}})^{\mathrm{T}}(\mathbf{K}_{\phi\phi}^{\mathrm{a}})^{-1}\mathbf{K}_{\phi\phi,1}^{\mathrm{a}}V^{k}. \tag{47}$$

2.7. Global governing equations of motion

The global system governing equations of motion derived from Eq. (35) in terms of the global coordinates with the standard procedure of the finite element method can be expressed as follows:

$$\mathbf{M}\ddot{\tilde{\mathbf{u}}} + (\mathbf{K}_{uu} + \mathbf{K}_{\mathrm{p}})\tilde{\mathbf{u}} = \mathbf{f} + \mathbf{f}_{\mathrm{a}}, \tag{48}$$

where $\tilde{\mathbf{u}}$ and $\ddot{\tilde{\mathbf{u}}}$ are the global coordinates representing the global nodal mechanical displacements and accelerations, respectively; $\mathbf{M}$ the global consistent mass matrix; $\mathbf{K}_{uu}$ the global mechanical stiffness matrix; $\mathbf{K}_{\mathrm{p}}$ the global induced stiffness matrix due to the piezoelectricity; $\mathbf{f}$ the global external mechanical forces; and $\mathbf{f}_{\mathrm{a}}$ the global equivalent mechanical forces of the applied voltages of the piezoelectric actuators. Since the unknown electric potentials of the finite sublayers of each piezoelectric layer have been condensed, it can be expected that the present FE model would not suffer from an excessive number of potential field variables in proportion to the number of piezoelectric layers and the number of sublayers as well as the size of the 2D mesh.

For the static analysis problems, $\ddot{\tilde{\mathbf{u}}} = 0$, the governing equations of motion in Eq. (48) reduces to

$$(\mathbf{K}_{uu} + \mathbf{K}_{\mathrm{p}})\tilde{\mathbf{u}} = \mathbf{f} + \mathbf{f}_{\mathrm{a}}. \tag{49}$$

For the dynamic frequency analysis problems, since $\mathbf{f} = 0$ and $\mathbf{f}_{\mathrm{a}} = 0$, the governing equations of motion in Eq. (48) reduces to

$$\mathbf{M}\ddot{\tilde{\mathbf{u}}} + (\mathbf{K}_{uu} + \mathbf{K}_{\mathrm{p}})\tilde{\mathbf{u}} = 0, \tag{50}$$

and the corresponding eigenvalue problem is:

$$|(\mathbf{K}_{uu} + \mathbf{K}_{\mathrm{p}}) - \omega^{2}\mathbf{M}| = 0, \tag{51}$$

where ω is the fundamental frequency.

3. Numerical results and discussion

In order to demonstrate the efficiency and accuracy of the present model in estimating both the global responses, such as the deflection and fundamental frequencies, and the local responses, such as the through-the-thickness variation of the electric potential, two examples are used in this study.

3.1. A PVDF bimorph beam

The PVDF bimorph piezoelectric beam proposed by Tzou and Tseng (1991) consists of two identical PVDF uniaxial beams with opposite polarities (see Fig. 3). The material properties of the PVDF extracted from Tzou and Tseng (1991) are shown in Table 1. The deflections of the bimorph cantilever beam at the specified nodes when a unit voltage (1 V) is applied across the thickness of the beam obtained by different methods are shown in Table 2, in which all the errors are with respect to the theory solution (Tzou and Tseng, 1991; Tzou, 1993). It can be seen that the results derived by the present FEM are in excellent agreement with available theoretical results, furthermore, the deflections derived by the present FEM (5 elements) are much closer to the theoretical solutions than those from the 3D FEM results of Tzou (1993) (10 elements) or those from the 1D FEM results of Shen (1994) (10 elements). Moreover, it can be seen that the results of the 3D FEM (isoparametric hexahedron solid element) developed by Tzou and Tseng (1990)

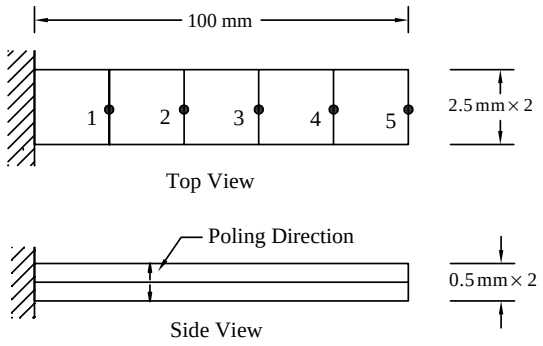

Fig. 3. A classical piezoelectric bimorph beam.

Table 1
Material properties of the PVDF

E_{11} (GPa)	E_{22} (GPa)	v	G_{12} (GPa)	ρ (kg/m^3)	d_{31} (C/N)	g_{33} (F/m)
2.0	2.0	0.29	0.775	1800	2.2×10^{-11}	1.062×10^{-10}

Table 2
Static deflection of the bimorph beam consisting of uniaxial PVDF materials (μm)

Node	1	2	3	4	5
Theory (Tzou, 1993)	0.0138	0.0552	0.124	0.221	0.345
3D FEM (Tzou, 1993)	0.0124	0.0508	0.116	0.210	0.330
Error (%)	−10.0	−8.0	−6.2	−5.1	−4.4
1D FEM (Shen, 1994)	0.0132	0.0528	0.1188	0.2112	0.330
Error (%)	−4.3	−4.3	−4.2	−4.4	−4.4
Present ($n_{sub} = 1$)	0.0134	0.054	0.122	0.218	0.342
Error (%)	−2.9	−2.2	−1.6	−1.4	−0.9
Present ($n_{sub} = 10$)	0.0132	0.054	0.121	0.218	0.341
Error (%)	−4.3	−2.2	−2.4	−1.4	−1.2

are not so close to the theory solution, especially at the nodes close to the fixed end, since the 3D model is relatively rigid (Shen, 1994) and less efficient for thin beams and plates due to the higher stiffness coefficients in the thickness direction (Hwang and Park, 1993). It can also be seen that the 1D FEM developed by Shen (1994) can well predict the deflections with errors within 4.4% since the piezoelectric bimorph beam itself can be simplified as a one-dimensional structure. It should be noted that the present FEM with 10 sublayer per PVDF layer does not assume a linear electric potential field distribution in the thickness. Since only slight difference in the deflection response can be observed while using this more accurate FE model, it can be concluded that the through-the-thickness distribution of the electric potential field can be assumed as linear. The reason can be that the relative thickness of the PVDF layers of this bimorph beam is so small (slenderness ratio is 100) that the nonlinear potentials induced by the electromechanical coupling in Eq. (45) of each PVDF actuator can be neglected.

3.2. A PZT bimorph plate

A piezoelectric bimorph plate (see Fig. 1) undergoing a surface density of normal force and electric potential applied to the top and bottom faces of the plate in (Fernandes and Pouget, 2003) is adopted. The

boundary conditions of this rectangular plate of length L and width ℓ are simple support. The bimorph is made of two identical layers of PZT-4 piezoelectric ceramics of which the material constants can be given (Ikeda, 1996; Fernandes and Pouget, 2003) as follows:

$$\mathbf{c} = \begin{bmatrix} 139 & 77.8 & 74.3 & 0 & 0 & 0 \\ 77.8 & 139 & 74.3 & 0 & 0 & 0 \\ 74.3 & 74.3 & 115 & 0 & 0 & 0 \\ 0 & 0 & 0 & 25.6 & 0 & 0 \\ 0 & 0 & 0 & 0 & 25.6 & 0 \\ 0 & 0 & 0 & 0 & 0 & 30.6 \end{bmatrix} \text{GPa}, \tag{52}$$

$$\mathbf{e} = \begin{bmatrix} 0 & 0 & 0 & 0 & 12.7 & 0 \\ 0 & 0 & 0 & 12.7 & 0 & 0 \\ -5.2 & -5.2 & 15.1 & 0 & 0 & 0 \end{bmatrix} \text{C/m}^2, \tag{53}$$

$$\mathbf{g} = \begin{bmatrix} 13.06 & 0 & 0 \\ 0 & 13.06 & 0 \\ 0 & 0 & 11.51 \end{bmatrix} \text{nF/m}. \tag{54}$$

The geometry of the plate is $L = 25$ mm and $\ell = 12.5$ mm and different slenderness ratios such as L/h =5, 10 and 50, in which h is the thickness of the piezoelectric bimorph plate, are considered. Two kinds of electromechanical loads are considered, corresponding to

(1) Sensor function with a force density per unit area $S_0 = 1000$ N/m^2 (linear load $P_s = S_0\ell$) applied to the upper face of the bimorph ($V_0 = 0$), where the numerical results are given in dimensionless units (Fernandes and Pouget, 2003) as

$$(W, \Phi) = \frac{c_{11}}{hS_0}(w, \phi/E_0) \tag{55}$$

in which c_{11} is the stiffness constant of elastic stiffness matrix (Eq. (52)), and the amplification factor E_0 is taken as $E_0 = 10^{10}$ m/V.

(2) Actuator function with an electric potential $V_0 = 50$ V applied to the top and bottom faces of the plate ($S_0 = 0$), where the numerical results are given in dimensionless units (Fernandes and Pouget, 2003) as

$$(W, \Phi) = \frac{E_0}{V_0}(w, \phi/E_0). \tag{56}$$

Fernandes and Pouget (2003) presented a Fourier series solution to this piezoelectric bimorph problem by adopting the plane strain assumption and used ABAQUS 2D plane strain elements to carry out the FE computations for comparison. However, full 3D analysis was not performed. As a further comparison in this study, in addition to the application of the present FE model (up to 200 elements), the ANSYS coupled-field analysis program ANSYS Multi-physics is used to carry out a full 3D analysis by considering the coupled-field brick elements (SOLID5) (up to 9600 elements are used) and the results from the full 3D FEM are taken as accurate in the present numerical comparison.

3.2.1. Piezoelectric sensor function

For this configuration a surface density of normal force is applied to the top surface of the bimorph and the piezoelectric layers are used as sensors in closed circuit, in which the top and bottom surfaces of the sensors are grounded. The through-the-thickness variation of both the deflection and the voltage in dimensionless unit at the plate center is shown in Fig. 4 for the aspect ratio $L/h = 10$. Fig. 4(a) shows that

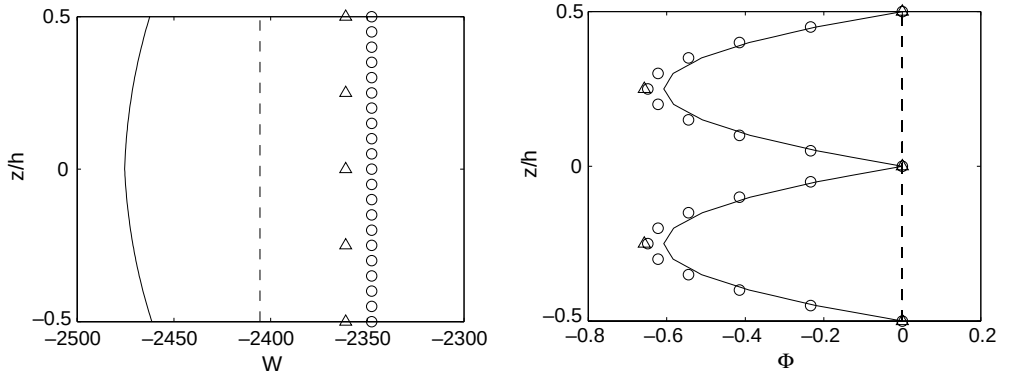

Fig. 4. Force density applied on the top surface of a PZT bimorph in closed circuit for $L/h = 10$. 3D FEM (full line), present ($n_{sub} = 1$) (dashed-line), present ($n_{sub} = 2$) (triangles) and present ($n_{sub} = 10$) (small circles).

the linear through-the-thickness variation of the deflection W predicted by the present model with different number of sublayers is a good approximation to the nonlinear variation predicted by the full 3D model. Furthermore, the deflections given by the present model are with smaller values than that of the 3D model, since the present FE model based on the plate theory (FOST) tends to overestimate the deflection stiffness of the plate. It can be expected that further refinement of the mesh could yield improved results. Among the deflections given by the present model, it can be seen that smaller deflection is obtained with the increase of the number of sublayers for each PZT layer. The reason can be that more constraints on the through-the-thickness electric potentials due to more sublayers involved would lead to a higher global stiffness. Fig. 4(b) shows that the through-the-thickness variation of the voltage Φ predicted by the present model with sublayers more than 1 can also be a good approximation to the nonlinear variation predicted by the full 3D model. More accurate approximation can be obtained by using more sublayers. Therefore, the present model can predict the actual through-the-thickness electric potential field well without adopting any prescribed higher-order through-the-thickness potential assumptions. It can also be observed that there is significant error in Φ when the linear electric potential model for the whole PZT layer is adopted, which will cause the induced potential of the piezoelectric sensors in closed circuit to vanish. Actually, the induced potential of the piezoelectric sensors in closed circuit has been ignored by a lot of researchers (Lee, 1990; Hanagud et al., 1992; Hwang and Park, 1993; Ray et al., 1994; Samanta et al., 1996; Lam et al., 1997; Yang, 1997; Aldraihem and Wetherhold, 1997; Lam and Ng, 1999; Auricchio et al., 2001; Wang et al., 2001; Wang, 2002; Zhu et al., 2002; Kapuria et al., 2003; Wang et al., 2004). However, according to the present study, it is suggested that all the piezoelectric models assuming the linear through-the-thickness electric potential distribution would be inaccurate to predict the local responses of the piezoelectric sensors.

Comparisons of the numerical results from the present model with different number of sublayers ($n_{sub} = 1$, 2 and 10) to those from the full 3D model and to those from the 2D plane strain model in (Fernandes and Pouget, 2003) are presented in Table 3 for three typical slenderness ratios ($L/h = 5$, 10 and 50), in which the 2D FEM and 2D analytical solutions (Fernandes and Pouget, 2003) are based on the plane strain assumption. The most interesting result is that the discrepancy between the maximum values of the deflection at the plate center for the present 2D bending model and the 2D plane strain model in (Fernandes and Pouget, 2003) is relatively small. The maximum estimating errors for the deflection is about 4.8% for $L/h = 50$, 5.2% for $L/h = 10$ and up to 9.7% for $L/h = 5$ (thick plate). However, the discrepancy for the maximum electric potential is up to 100% for all the three slenderness ratios. Hence, it can be

Table 3
Piezoelectric bimorph in closed circuit, applied surface density force

L/h	Approaches	W_{max}	Error(%)	Φ_{max}	Error(%)
5	3D FEM	176.22		0.154	
	Present ($n_{sub} = 10$)	162.49	7.8	0.161	4.6
	Present ($n_{sub} = 2$)	163.31	7.3	0.163	5.8
	Present ($n_{sub} = 1$)	166.02	5.8	0	100
	2D FEM	159.21	9.7	0.197	27.9
	2D Analytical	161.47	8.4	0.206	33.8
10	3D FEM	2475.5		0.607	
	Present ($n_{sub} = 10$)	2347.8	5.2	0.648	6.8
	Present ($n_{sub} = 2$)	2361.1	4.6	0.657	8.2
	Present ($n_{sub} = 1$)	2405.5	2.8	0	100
	2D FEM	2349.4	5.1	0.766	26.2
	2D Analytical	2358.4	4.7	0.775	27.7
50	3D FEM	1.4844×10^6		15.66	
	Present ($n_{sub} = 10$)	1.4128×10^6	4.8	16.40	4.7
	Present ($n_{sub} = 2$)	1.4214×10^6	4.2	16.63	6.2
	Present ($n_{sub} = 1$)	$1.4498\times10_6$	2.3	0	100
	2D FEM	1.4285×10^6	3.8	18.98	21.2
	2D Analytical	1.4287×10^6	3.8	18.99	21.3

concluded that the local responses such as the induced electric potentials of the piezoelectric sensors in Eq. (39) would not affect the global responses such as the deflection of the plate significantly since the top and bottom surfaces of the sensors are grounded, as shown in Eq. (38). Therefore, it should be highlighted that piezoelectric models of (Lee, 1990; Hanagud et al., 1992: Hwang and Park, 1993; Ray et al., 1994; Samanta et al., 1996; Lam et al., 1997; Yang, 1997; Aldraihem and Wetherhold, 1997; Lam and Ng, 1999; Auricchio et al., 2001; Wang et al., 2001; Wang, 2002; Zhu et al., 2002; Kapuria et al., 2003; Wang et al., 2004) based on the linear through-the-thickness electric potential distribution assumption may be able to provide good approximate results for the global responses, especially when the bimorph plate is thin or moderately thick, though the induced potentials are not accurately estimated. Furthermore, it should be noted that the 2D plane strain model in (Fernandes and Pouget, 2003) can also predict the deflection of thin or moderately thick bimorph plates well, since the plate with an aspect ratio L/ℓ of 2 and a uniformly distributed surface density force can be approximated as unidirectional and the induced electric potentials are insignificant.

3.2.2. Piezoelectric actuator function

For this configuration the piezoelectric bimorph plate is subject to an electric potential $V_0 = 50$ V applied to the bottom and top surfaces of the plate and the intermediate electrode is set to zero voltage (see Fig. 1). The through-the-thickness variation of both the deflection and the voltage in dimensionless unit at the plate center is shown in Fig. 5 for the aspect ratio $L/h = 10$. Fig. 5(a) shows that the linear through-the-thickness variation of the deflection W predicted by the present model with different number of sublayers is a good approximation to the nonlinear variation predicted by the full 3D model and the deflection value becomes smaller as the number of sublayers for each PZT layer increases, similar to the previous observation. Fig. 5(b) shows the interesting result that the through-the-thickness variation of the voltage Φ predicted by the present model with different number of sublayers can all be a good approximation to the nonlinear variation predicted by the full 3D model and the through-the-thickness distribution of the electric potential field can be well approximated as linear, as shown in dashed line in Fig. 5(b). The reason can be that the

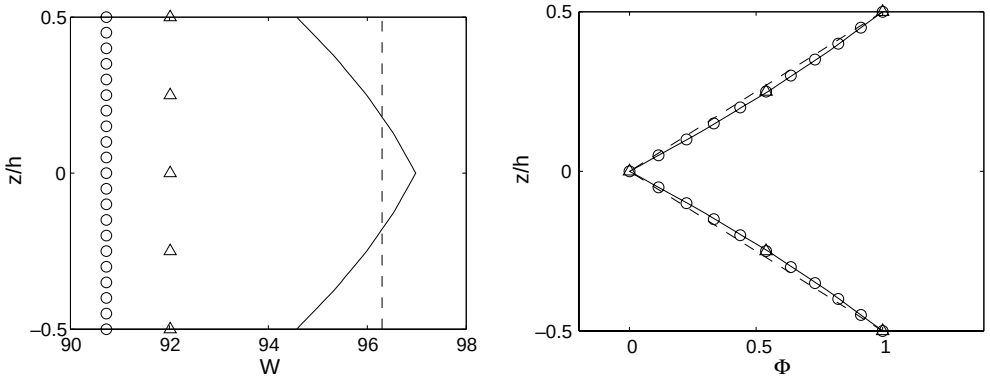

(a) Dimensionless W (b) Dimensionless Φ

Fig. 5. Electric potential applied to a piezoelectric bimorph for $L/h = 10$.

nonlinear induced electric potentials in Eq. (45) is insignificant compared to the applied linear electric potentials for thin or moderately thick plates, as discussed in detail in Section 2.6.3.

Furthermore, comparisons of the numerical results from the present model with different number of sublayers ($n_{\text{sub}} = 1$, 2 and 10) to those from the full 3D model and to those from the 2D plane strain model in (Fernandes and Pouget, 2003) are made in Table 4 for three slenderness ratios ($L/h = 5$, 10 and 50), in which $\Phi_m = \Phi(L/2, \ell/2, -h/4)$. Again, the linear through-the-thickness electric potential model ($n_{\text{sub}} = 1$) demonstrates its efficiency in predicting the global response deflection W with the maximum error of 1.7% for all the three slenderness ratios, though the error for the local response electric potential Φ_m is about 8.4% for $L/h = 50$, 8.6% for $L/h = 10$ and up to 9.1% for $L/h = 5$ (thick plate). Furthermore,

Table 4
Electric potential applied to a piezoelectric bimorph

L/h	Approaches	$W_{\max}$	Error(%)	Φ_m	Error(%)
5	3D FEM	23.454		0.550	
	Present ($n_{\text{sub}} = 10$)	22.439	4.3	0.542	1.5
	Present ($n_{\text{sub}} = 2$)	22.763	3.0	0.542	1.5
	Present ($n_{\text{sub}} = 1$)	23.840	1.7	0.5	9.1
	2D FEM	26.197	11.7	–	–
	2D Analytical	27.654	17.9	–	–
10	3D FEM	97.0		0.547	
	Present ($n_{\text{sub}} = 10$)	90.7	6.5	0.539	1.5
	Present ($n_{\text{sub}} = 2$)	92.0	5.2	0.540	1.3
	Present ($n_{\text{sub}} = 1$)	96.3	0.7	0.5	8.6
	2D FEM	115.5	19.1	–	–
	2D Analytical	116.0	19.6	–	–
50	3D FEM	2477.8		0.546	
	Present ($n_{\text{sub}} = 10$)	2298.5	7.2	0.536	1.8
	Present ($n_{\text{sub}} = 2$)	2330.5	5.9	0.536	1.8
	Present ($n_{\text{sub}} = 1$)	2436.6	1.7	0.5	8.4
	2D FEM	2943.9	18.8	–	–
	2D Analytical	2943.3	18.8	–	–

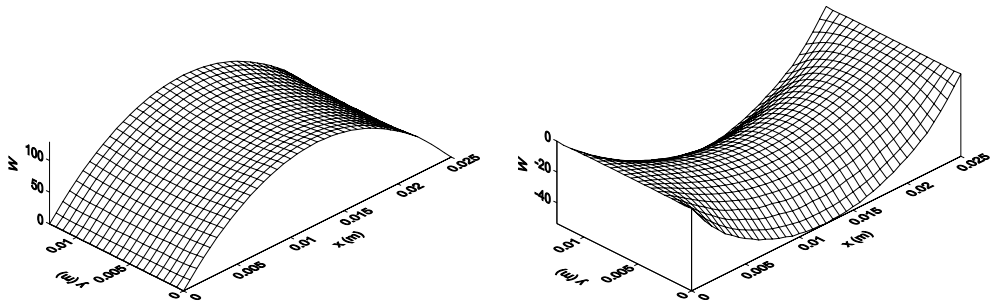

(a) $e_{31} \neq 0,\ e_{32} = 0$ (b) $e_{31} = 0,\ e_{32} \neq 0$

Fig. 6. Effect of the piezoelectric constants on the deflection of the bimorph plate subject to an electric voltage for $L/h = 10$.

it should be noted that the discrepancy for the maximum deflection $W_{\max}$ given by the present FE model for the thick plate $L/h = 5$ is relatively small. The reason can be that the FOST plate theory may overestimate the global stiffness of the thick plate such that the equivalent actuator forces in Eq. (47) would also become larger. More importantly, it is shown in Table 4 that the discrepancy for the maximum deflection $W_{\max}$ given by the 2D plane strain model in (Fernandes and Pouget, 2003) for all the three slenderness ratios is always significant. The maximum estimating errors for the deflection is about 18.8% for $L/h = 50$, 19.6% for $L/h = 10$ and 17.9% for $L/h = 5$. In those plane models (Shen, 1994; Gopinathan et al., 2000; Wang and Quek, 2002; Kapuria, 2001; Fernandes and Pouget, 2003), the contribution of the extension of the piezoelectric actuators due to the piezoelectric constant e_{32} to the global responses is ignored while the piezoelectric material PZT is adopted as actuators. However, PZT actuator is naturally isotropic in the plane of operation (Aldraihem and Wetherhold, 1997), i.e. $e_{31} = e_{32}$. Hence, the issue whether the contribution of the extension due to e_{32} to the global responses is significant should be addressed by those plane models. Based on the present 2D bending model, Fig. 6 shows the effect of the piezoelectric constants on the deflection of the bimorph plate subject to the electric voltage for $L/h = 10$. It can be seen that for the case $e_{31} = 0$ and $e_{32} \neq 0$ the plate deflect in a direction opposite to that of the case $e_{31} \neq 0$ and $e_{32} = 0$ due to the boundary conditions on the plate contour. Those plane models can evaluate the contribution of the extension due to e_{31} to the deflection, as shown in Fig. 6(a), but the deflection due to e_{32} as shown in Fig. 6(b) is ignored. However, this deflection is not insignificant in this study. Actually, the deflection response of the bimorph plate predicted by the present model, which is approximately the superposition of the deflections in Fig. 6(a) and (b), is significantly smaller (about 20% in the central deflection) than that predicted by the 2D plane strain model without considering the electromechanical coupling effect of e_{32}. Therefore, those plane models would be considered as inappropriate and less accurate in estimating the global responses to an electric potential applied to PZT actuators unless the electromechanical effect of e_{32} is taken into account or proved to be less significant due to the specified boundary conditions or material properties.

3.2.3. Vibration of the piezoelectric bimorph

In this section, modal frequencies of the piezoelectric bimorph plate structure for both the open circuit and closed circuit conditions on the top and bottom surfaces of the piezoelectric layers for the typical slenderness ratio $L/h = 10$ are studied. The first six modes of the bimorph plate are shown in Fig. 7. It can be seen that only the flexural modes 3 and 6 may be accurately predicted and all the other modes among them will be missed by the plane strain model (Fernandes and Pouget, 2003). Therefore, it should be noted that the plane strain model in (Fernandes and Pouget, 2003) can only give approximate predictions to the modal frequencies of the bimorph plate.

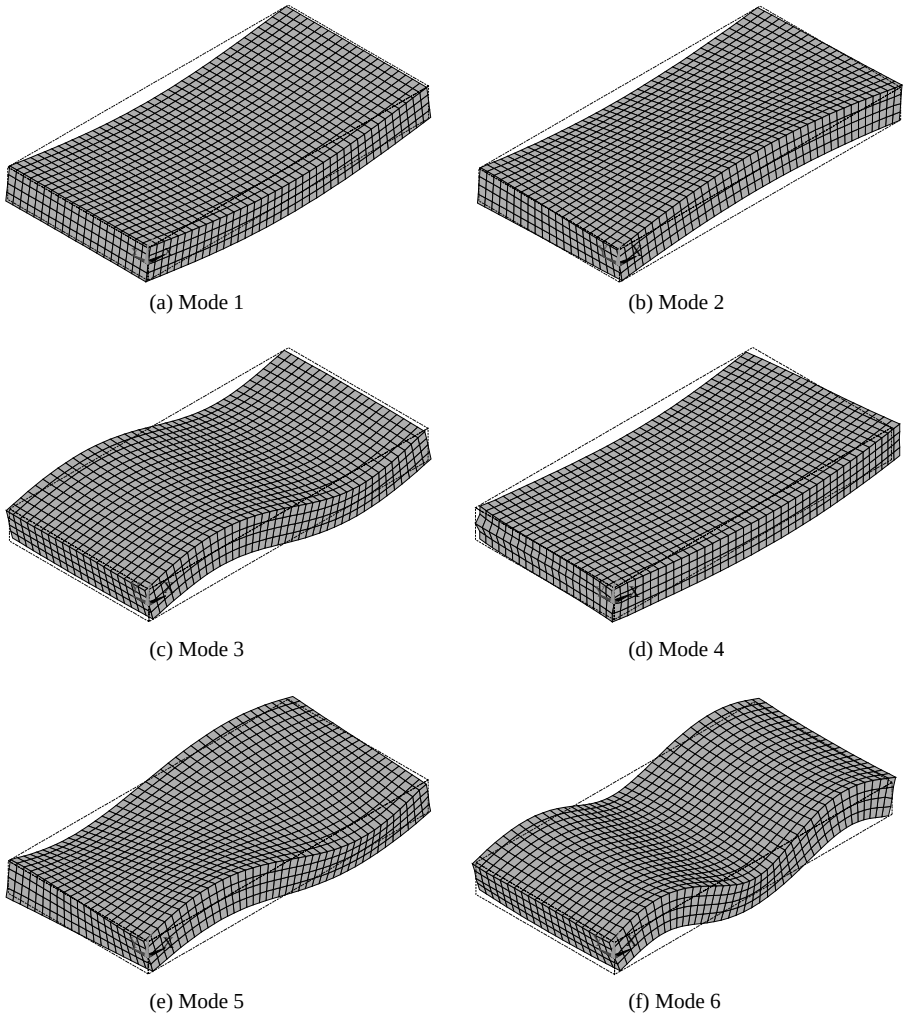

(a) Mode 1 (b) Mode 2

(c) Mode 3 (d) Mode 4

(e) Mode 5 (f) Mode 6

Fig. 7. Shapes of the first six modes of the bimorph plate for $L/h = 10$.

The modal frequencies of the bimorph plate predicted by the present model are shown in Tables 5 and 6 in comparison to the corresponding results given by the full 3D model and the 2D plane strain model (Fernandes and Pouget, 2003). It is shown that the results from the present model with different number of sublayers all agree well with those from the full 3D model (maximum error is 6.1%), which suggests that the through-the-thickness electric potential distribution does not affect the global modal frequencies much for the thin and moderately thick piezoelectric plates. This observation is also consistent with a recent observation based on a new 3D piezoelectric model proposed by Yao and Lu (2003). It can also be seen that the frequency of the fourth mode remains unchanged for different number of sublayers used for each PZT layer. This can be explained by the fact that this mode is an inplane shear mode and the transversally isotropic PZT cannot produce shear deformations to affect this mode, as discussed in detail in (Aldraihem and Wetherhold, 1997; Wang et al., 2003). Furthermore, the value of each modal frequency for the piezoelectric bimorph plate in closed circuit is always smaller than that in open circuit. The reason is that the induced stiffness of the latter is higher since the induced electric potential field in the open circuit is less

Table 5
Modal frequencies (Hz) for the piezoelectric bimorph plate in closed circuit ($L/h = 10$)

Modes	1	2	3	4	5	6
3D FEM	6055	14,605	23,276	25,220	33,990	48,941
Present ($n_{sub} = 10$)	6258	13,833	23,814	26,612	33,057	49,664
Error (%)	3.4	5.3	2.3	5.5	2.7	1.5
Present ($n_{sub} = 2$)	6242	13,827	23,754	26,612	33,020	49,554
Error (%)	3.1	5.3	2.1	5.5	2.9	1.3
Present ($n_{sub} = 1$)	6190	13,804	23,561	26,612	32,902	49,197
Error (%)	2.2	5.5	1.2	5.5	3.2	0.5
2D FEM	–	15,747	–	–	–	59,370
Error (%)	–	7.8	–	–	–	21.3
2D Analytical	–	15,769	–	–	–	59,677
Error (%)	–	8.0	–	–	–	21.9

Table 6
Modal frequencies (Hz) for the piezoelectric bimorph plate in open circuit ($L/h = 10$)

Modes	1	2	3	4	5	6
3D FEM	6141	14,634	23,575	25,407	34,114	49,381
Present ($n_{sub} = 10$)	6433	13,909	24,473	26,967	33,452	50,880
Error (%)	4.8	5.0	3.8	6.1	1.9	3.0
Present ($n_{sub} = 2$)	6420	13,904	24,425	26,967	33,424	50,792
Error (%)	4.5	5.0	3.6	6.1	2.0	2.9
Present ($n_{sub} = 1$)	6379	13,886	24,272	26,967	33,332	50,509
Error (%)	3.9	5.1	3.0	6.1	2.3	2.3
2D FEM	–	16,656	–	–	–	62,024
Error (%)	–	13.8	–	–	–	25.6
2D Analytical	–	16,681	–	–	–	62,375
Error (%)	–	14.0	–	–	–	26.3

constrained, as discussed in Section 2.6.2. As a comparison, it can be seen that the frequencies of the flexural modes predicted by the 2D plane strain model (Fernandes and Pouget, 2003) are significantly higher than those predicted by the full 3D model since the flexural modes assumed by the 2D plane strain model tends to overestimate the global flexural stiffness of the actual 2D bimorph plate.

4. Conclusions

An efficient finite element model that combines finite 2D single-layer elements with finite 3D piezoelectric sublayer elements has been proposed for the static and dynamic analysis of a piezoelectric bimorph. The actual through-the-thickness electric potential distribution can be accurately predicted with a linear distribution assumption for each piezoelectric sublayer. According to the present model, the nonlinear induced electric potentials of piezoelectric sensors in closed circuit is insignificant for thin or moderately thick bimorph plates. The higher induced electric potentials of bimorph sensors in open circuit would lead to a higher induced stiffness and a higher global frequency response. Furthermore, the nonlinear induced electric potentials of piezoelectric actuators are inferior to the directly applied linear electric potentials. The present model has been verified by good agreement in numerical solutions with a full 3D model. It is shown that the present model with even $n_{sub} = 2$ can achieve good predictions in both the global and local responses and the conventional linear through-the-thickness potential assumption can only predict the global

response well. Further evaluation on a 2D plane strain model for a transversally isotropic PZT bimorph plate has been performed and it is shown that the model may be less accurate in predicting the static response to an electric loading and the global frequency response and thus further improvements are recommended. The present study can be of importance for researchers to establish more accurate and efficient piezoelectric models based on better understanding to the piezoelectricity.

References

Aldraihem, O.J., Wetherhold, R.C., 1997. Mechanics and control of coupled bending and twisting vibration of laminated beams. Smart Materials and Structures 6 (1), 123–133.

Auricchio, F., Bisegna, P., Lovadina, C., 2001. Finite element approximation of piezoelectric plates. International Journal for Numerical Methods in Engineering 50 (6), 1469–1499.

Bisegna, P., Caruso, G., 2001. Evaluations of higher-order theories of piezoelectric plates in bending and in stretching. International Journal of Solids and Structures 38 (48–49), 8805–8830.

Bisegna, P., Maceri, F., 1996. An exact three-dimensional solution for simply supported rectangular piezoelectric plate. ASME Journal of Applied Mechanics 63, 628–638.

Cheng, D.K., 1989. Field and Wave Electromagnetics, 2nd Edition. Addison-Wesley Publishing Co., Inc., Reading Mass.

Ehlers, S.M., Weisshaar, T.A., 1990. Static aeroelastic behavior of an adaptive laminated piezoelectric composite wing. AIAA Journal 28 (4), 1611–1623.

Fernandes, A., Pouget, J., 2003. Analytical and numerical approaches to piezoelectric bimorph. International Journal of Solids and Structures 40 (17), 4331–4352.

Gopinathan, S.V., Varadan, V.V., Varadan, V.K., 2000. A review and critique of theories for piezoelectric laminates. Smart Materials and Structures 9 (1), 24–48.

Ha, S.K., Kim, Y.H., 2002. Analysis of a piezoelectric multi-morph in extentional and flexural motions. Journal of Sound and Vibration 253 (5), 1001–1014.

Hanagud, S., Obal, M.W., Calise, A.J., 1992. Optimal vibration control by the use of piezoceramic sensors and actuators. Journal of Guidance, Control, and Dynamics 15 (5), 1199–1206.

Hughes, T.J.R., 1987. The Finite Element Method: Linear Static and Dynamic Finite Element Analysis. Prentice-Hall, Inc., Englewood Cliffs.

Hwang, W.S., Park, H.C., 1993. Finite element modeling of piezoelectric sensors and actuators. AIAA Journal 31 (5), 930–937.

Ikeda, T., 1996. Fundamental of Piezoelectricity. Oxford University Press, Oxford, U.K.

Kapuria, S., 2001. An efficient coupled theory for multilayered beams with embedded piezoelectric sensory and active layers. International Journal of Solids and Structures 38 (50–51), 9179–9199.

Kapuria, S., Dube, G.P., Dumir, P.C., 2003. First-order shear deformation theory solution for a circular piezoelectric composite plate under axisymmetric load. Smart Materials and Structures 12 (3), 417–423.

Kekana, K., 2002. Finite element modeling of laminated piezo-elastic structures: Lypunov stability analysis. Journal of Sound and Vibration 256 (3), 463–473.

Lam, K.Y., Ng, T.Y., 1999. Active control of composite plates with integrated piezoelectric sensors and actuators under various dynamic loading conditions. Smart Materials and Structures 8 (2), 223–237.

Lam, K.Y., Peng, X.Q., Liu, G.R., Reddy, J.N., 1997. A finite-element model for piezoelectric composite laminates. Smart Materials and Structures 6 (5), 583–591.

Lee, C.K., 1987. Piezoelectric laminates for torsional and bending modal control: Theory and experiment. Ph.D. Dissertation, Cornell University.

Lee, C.K., 1990. Theory of laminated piezoelectric plates for the design of distributed sensors/actuators. Part I: Governing equations and reciprocal relationships. Journal of Acoustic Society of America 87 (3), 1144–1158.

Lee, P.C.Y., Lin, W.S., 1998. Piezoelectrically forced vibrations of rectangular SC-cut quartz plates. Journal of Applied Physics 83 (12), 7822–7833.

Mackerle, J., 2003. Smart materials and structures—a finite element approach—an addendum: a bibliography (1997–2002). Modelling and Simulation in Materials Science and Engineering 11, 707–744.

Mindlin, R.D., 1952. Forced thickness-shear and flexural vibrations of piezoelectric crystal plates. Journal of Applied Physics 23, 83–88.

Mindlin, R.D., 1972. High frequency vibrations of piezoelectric crystal plates. International Journal of Solids and Structures 8 (6), 895–906.

Ray, M.C., Bhattacharya, R., Samanta, B., 1993. Exact solutions for static analysis of intelligent structures. AIAA Journal 31 (9), 1684–1691.

Ray, M.C., Bhattacharya, R., Samanta, B., 1998. Exact solutions for dynamic analysis of composite plates with distributed piezoelectric layers. Computers and Structures 66 (6), 737–743.

Ray, M.C., Bhattacharyya, R., Samanta, B., 1994. Static analysis of an intelligent structure by the finite element method. Computers and Structures 52 (4), 617–631.

Reddy, J.N., 1997. Mechanics of Laminated Composite Plates: Theory and Analysis. CRC Press, Boca Raton.

Samanta, B., Ray, M.C., Bhattacharyya, R., 1996. Finite element model for active control of intelligent structures. AIAA Journal 34 (9), 1885–1893.

Saravanos, D.A., Heyliger, P.R., Hopkins, D.A., 1997. Layerwise mechanics and finite element for the dynamic analysis of piezoelectric composite plates. International Journal of Solids and Structures 34 (3), 359–378.

Shen, M.-H.H., 1994. Analysis of beams containing piezoelectric sensors and actuators. Smart Materials and Structures 3 (4), 439–447.

Tiersten, H.F., 1993. Equations for the extension and flexure of relatively thin electroelastic plates under large electric fields. In: Lee, J.S. (Ed.), Mechanics of Electromagnetic Materials and Structures, vol. 161. ASME AMD, New York, pp. 21–34.

Tzou, H.S., 1993. Piezoelectric shells. In: Solid Mechanics and Its Applications, vol. 19. Kluwer Academic Publishers, Dordrecht.

Tzou, H.S., Tiersten, H.F., 1994. Elastic analysis of laminated composite plates in cylindrical bending due to piezoelectric actuators. Smart Materials and Structures 3 (3), 255–265.

Tzou, H.S., Tseng, C.I., 1990. Distributed piezoelectric sensor/actuator design for dynamic measurement/control of distributed parameter systems: A piezoelectric finite element approach. Journal of Sound and Vibration 138 (1), 17–34.

Tzou, H.S., Tseng, C.I., 1991. Distributed vibration control and identification of coupled elastic/piezoelectric systems: finite element formulation and applications. Mechanical Systems and Signal Processing 5 (3), 215–231.

Wang, S.Y., 2002. Active vibration control of smart piezoelectric composite plates. Ph.D. Dissertation, National University of Singapore, Singapore.

Wang, S.Y., Ang, K.K., Quek, S.T., 1999. Finite element modeling of smart composite plates. In: Wang, C.M., Lee, K.H., Ang, K.K. (Eds.), Solid Mechanics and Fluid Mechanics. Computational Mechanics for the Next Millenium, vol. 1. Proceedings of APCOM '99. Elsevier Science Ltd., Oxford, UK, pp. 267–272.

Wang, Q., Quek, S.T., 2002. A model for the analysis of beams with embedded piezoelectric layers. Journal of Intelligent Material Systems and Structures 13 (1), 61–70.

Wang, S.Y., Quek, S.T., Ang, K.K., 2001. Vibration control of smart piezoelectric composite plates. Smart Materials and Structures 10 (4), 637–644.

Wang, S.Y., Quek, S.T., Ang, K.K., 2004. Dynamic stability analysis of finite element modeling of piezoelectric composite plates. International Journal of Solids and Structures 41 (3–4), 745–764.

Wang, S.Y., Tai, K., Quek, S.T., 2003. Topology optimization of piezoelectric sensors/actuators for torsional vibration control of composite plates. Journal of Sound and Vibration, submitted for publication.

Yang, J.S., 1997. Equations for the flexural motion of elastic plates with partially electroded piezoelectric actuators. Smart Materials and Structures 6 (4), 485–490.

Yang, J.S., 1999. Equations for thick elastic plates with partially electroded piezoelectric actuators and higher order electric fields. Smart Materials and Structures 8 (1), 73–82.

Yao, L.Q., Lu, L., 2003. Hybrid-stabilized solid-shell model of laminated composite piezoelectric structures under non-linear distribution of electric potential through thickness. International Journal for Numerical Methods in Engineering 58 (10), 1499–1522.

Zhu, M.L., Lee, S.-W.R., Li, H.L., Zhang, T.Y., Tong, P., 2002. Modeling of torsional vibration induced by extension–twisting coupling of anisotropic composite laminates with piezoelectric actuators. Smart Materials and Structures 11 (1), 55–62.